


Magnetization coupling in a YIG/GGG structure

Ledong Wang, Zhijian Lu, Xiaonan Zhao, Weizhen Zhang, Yanxue Chen, Yufeng Tian, Shishen Yan, and Lihui Bai *

School of Physics, State Key Laboratory of Crystal Materials, Shandong University, 27 Shandan Road, Jinan 250100, China

Michael Harder

Department of Physics, British Columbia Institute of Technology, 3700 Willingdon Avenue, Burnaby, British Columbia, Canada V5G 3H2



(Received 27 November 2019; revised 11 July 2020; accepted 30 September 2020; published 20 October 2020)

We studied the magnetization coupling between an yttrium-iron-garnet (YIG) film and a gadolinium-gallium-garnet (GGG) substrate at low temperature using magnetic resonance measurements. We observed both acoustic and optical mode hybridization between the magnetization of the 3- μm -thick YIG film, M_{YIG} , and the magnetization of the GGG substrate, M_{GGG} , corresponding to in-phase and out-of-phase coupling, respectively. This experimental observation can be described by an antiferromagnetic-type interaction between M_{YIG} and M_{GGG} in the Landau-Lifshitz-Gilbert equation. Taking this approach we find that the effective field induced by magnetization coupling can be enhanced by decreasing the temperature or increasing the external field, providing a means to control magnon dynamics in YIG for magnonic device applications.

DOI: [10.1103/PhysRevB.102.144428](https://doi.org/10.1103/PhysRevB.102.144428)

I. INTRODUCTION

Quantized spin waves, known as magnons, play an increasingly important role in quantum information technologies [1–7], requiring magnon manipulation techniques to store, extract, and transmit information. Magnon dynamics and manipulation in yttrium iron garnet [$\text{Y}_3\text{Fe}_5\text{O}_{12}$ (YIG)] is especially important, owing to the fact that YIG can be fabricated as a high-quality thin film with exceptionally low Gilbert damping of $\alpha = 10^{-5}$ [8], extending magnon lifetimes and propagation lengths. Attempts have been made to control YIG magnons by optimizing the YIG film surface structure [9–14], and while they have had some success in magnon-based information transfer, these techniques also lead to defects in the YIG film, reducing the magnon coherence length. Photonic manipulation of YIG magnons has also been demonstrated experimentally via strong coupling to a microwave cavity [15–20], and recently observed in nanomagnonic devices [21,22]. However, cavity quality is often a limiting factor, introducing more losses than magnon damping, thereby limiting coherent information transfer. Therefore the development of new magnon control methods, in particular those based on magnon-magnon interactions, is key to designing YIG-based magnonic devices.

Recently, interlayer mediated magnetization interactions between two adjacent nanomagnetic layers have been reported in a YIG/Co bilayer [23] and a Ni/YIG/Ni structure [24]. Sublattice coupling in layered CrCl_3 crystals [25], as well as crystals of the compensated ferrimagnet $\text{Gd}_3\text{Fe}_5\text{O}_{12}$ [26], has also been reported. The coupling between layered structures has great potential for magnonic device applications since the magnetization coupling may be controlled by manipulating

the interlayer interaction. In this vein it is fruitful to carefully study the coupling between YIG and gadolinium-iron-garnet (GGG), which is already widely used as a growth substrate for YIG films [27,28] due to their similar lattice constants. GGG substrates have a large paramagnetism, especially at low temperatures, suggesting that the coupling between YIG and GGG magnetization could be used to control magnon dynamics in YIG thin films.

In this work, we studied the temperature-controlled magnetization coupling between a YIG layer and GGG substrate using magnetic resonance absorption. We experimentally observed an interaction between the YIG magnetization, M_{YIG} , and the GGG magnetization, M_{GGG} , resulting in acoustic modes when the YIG and GGG magnetic resonances were in phase, and optical modes when they were π out of phase. Below 30 K, when the GGG paramagnetism is comparable to the YIG magnetization, the resonance field of the optical mode shifts rapidly to higher fields due to a difference in the magnetization temperature dependence compared to the YIG crystal, as expected according to Bloch's law [29]. This experimental behavior can be described by including an antiferromagnetic-type interaction between M_{GGG} and M_{YIG} in the Landau-Lifshitz-Gilbert (LLG) equation, demonstrating that magnons in the YIG film are controlled by the magnetization coupling. The effective field can be further enhanced by decreasing the temperature and increasing the external magnetic field, which may be helpful in the design of future magnonic devices.

II. EXPERIMENTAL METHODS

Our YIG/GGG bilayer consisted of a 3- μm -thick YIG layer deposited on a GGG substrate using liquid phase deposition, with lateral dimensions of 3 mm \times 6 mm. This device was placed in a cryogenic chamber for low-temperature

*lhbai@sdu.edu.cn

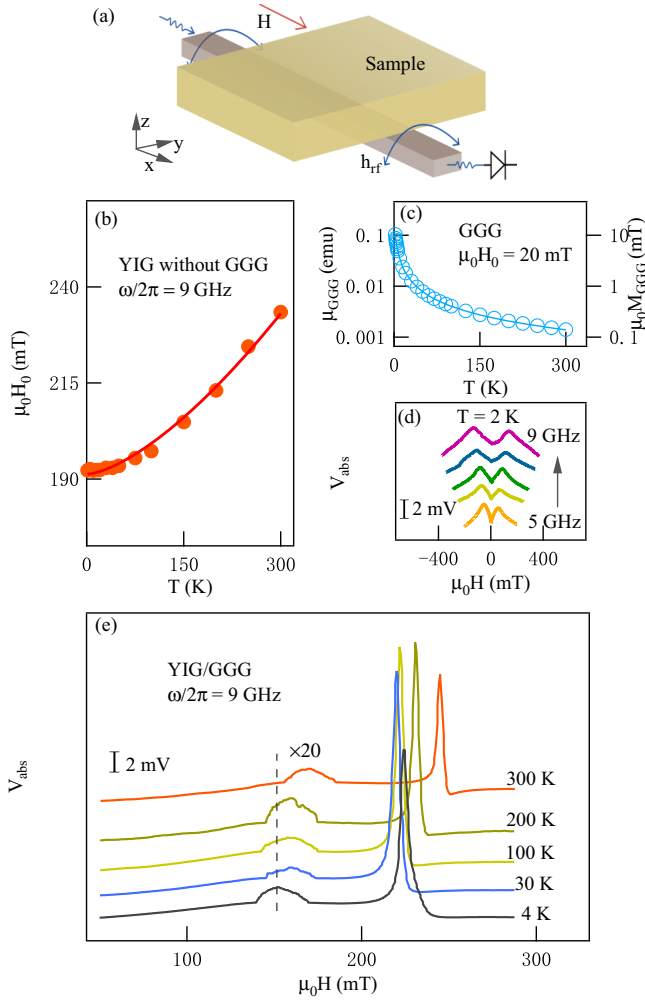


FIG. 1. (a) Schematic illustration of the microwave absorption measurement setup. An external magnetic field H is applied along the conductive strip in which microwaves propagate (x axis). (b) Resonance field $\mu_0 H_0$ of a pure YIG crystal and (c) M_{GGG} of a pure GGG substrate, are plotted as a function of measurement temperatures. Here the three-dimensional size of the GGG substrate is $5 \text{ mm} \times 5 \text{ mm} \times 0.5 \text{ mm}$. (d) Waterfall plot of the magnetic resonance absorption spectrum in the GGG substrate. The spectra correspond to microwave frequencies from 5 to 9 GHz, at 1 GHz intervals, and were measured at 2 K. The spectra are offset for clarity. (e) Waterfall plot of the magnetic resonance absorption spectrum at various temperatures in YIG/GGG. The spectra were measured at $\omega/2\pi = 9 \text{ GHz}$ and are offset for clarity. The low-field resonance mode at each temperature is magnified by a factor of 20.

measurements of the magnetization dynamics. To compare to the YIG/GGG bilayer, an identical GGG substrate ($5 \text{ mm} \times 5 \text{ mm} \times 0.5 \text{ mm}$, $\langle 111 \rangle$ orientation) and a single-crystal YIG disk (diameter = 5 mm , thickness = 0.5 mm), were measured under resonance conditions as reference samples. At room temperature the magnetic resonance properties of the YIG crystal are similar to that in the YIG/GGG bilayer as shown in Figs. 1(b) and 2.

Our experimental setup is shown in Fig. 1(a). The microwave field used to drive magnetic resonance, h_{rf} , is supplied by a coplanar waveguide, and an external magnetic

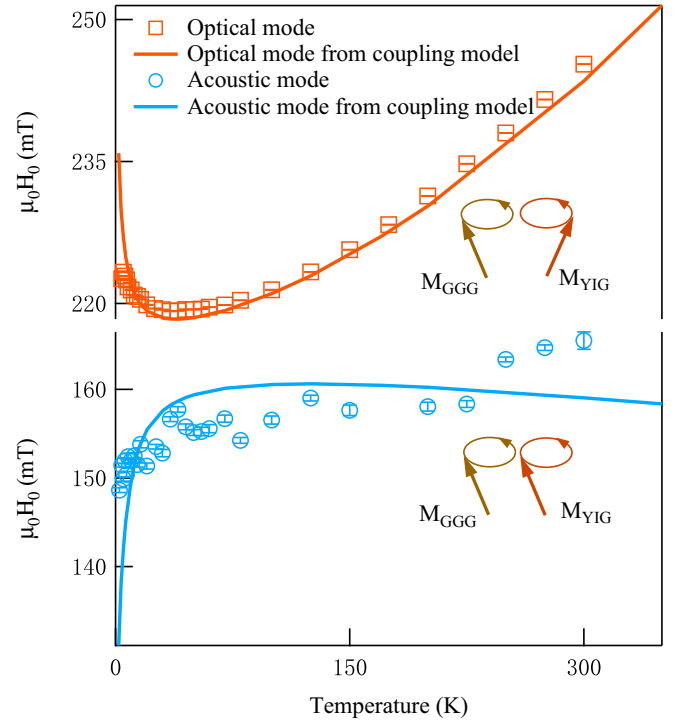


FIG. 2. The experimental resonance fields $\mu_0 H_0$ of the optical mode and the acoustic mode in the YIG/GGG structure compared to the magnetization coupling model. Arrows indicate the classical precession of M_{YIG} and M_{GGG} . Here the microwave frequency is 9 GHz.

field, H , is applied in the x direction, perpendicular to the h_{rf} plane. We used a microwave output power of 100 mW modulated at 8.33 kHz to perform lock-in measurements and the microwave transmission intensity was detected as a DC voltage, V_{abs} , through a diode.

As a reference, the paramagnetism of a pure GGG substrate was measured using a superconducting quantum interference device (SQUID) and the magnetic resonance in the YIG film was also electrically detected via spin pumping using a platinum (Pt) detector partially ($200 \mu\text{m} \times 20 \mu\text{m}$) sputtered on top of the YIG layer. The Pt layer has a thickness of 3 nm, which is slightly larger than its spin diffusion length [30–32]. The spin pumping and the magnetic resonance absorption were measured simultaneously using two lock-in amplifiers. The base pressure and sputtering pressure for magnetron sputtering of the Pt layer were 2×10^{-5} and 0.68 Pa, respectively.

III. RESULTS AND DISCUSSION

A. Magnetism in YIG and in GGG

The magnetism of YIG, and its temperature-dependent magnetic properties, has been widely studied theoretically and experimentally [33–38]. In a Pure YIG crystal the ferromagnetic resonance (FMR) field, $\mu_0 H_0$, follows a Kittel dispersion $(\omega/\gamma)^2 = \mu_0^2 H_0 (H_0 + M)$ [39]. Here M is the saturation magnetization of the YIG crystal, which usually varies with temperature T following Bloch's law $M(T) \propto -T^{3/2}$ [29]. Thus $\mu_0 H_0$ of the pure YIG layer will increase with increasing T for a fixed microwave

frequency ω , as shown in Fig. 1(b), where circles are experimental results and the line is calculated from Bloch's law and Kittel's dispersion.

As shown in Fig. 1(c), the temperature-dependent paramagnetism in a pure GGG substrate leads to a rapid increase in GGG magnetization, $\mu_0 M_{GGG}$, at low temperatures. As a result magnetic resonance measurements can be performed, as shown in Fig. 1(d) at $T = 2$ K for various microwave frequencies (4–9 GHz). A Gilbert damping of $\alpha_{GGG} = 0.036$ was determined by analyzing the frequency-dependent line width, $\Delta H(\omega)$ from Fig. 1(d), and the gyromagnetic ratio, $\gamma_{GGG} = 2\pi \times 59$ GHz/T, was determined by fitting the ω - H dispersion. Based on this large magnetic response, coupling between the YIG and GGG magnetizations would be expected in a YIG/GGG structure.

In Fig. 1(e) we summarize the magnetic resonance absorption spectra measured in YIG/GGG at different measurement temperatures from 300 to 4 K. These spectra reveal two resonance modes. We find that the resonance field, H_0 , of the high-field mode decreases as the temperature is lowered, reaching a minimum value near $T = 40$ K. Below 40 K, H_0 of the high-field mode increases, while H_0 of the low-field mode decreases. Similar behavior was observed at other microwave frequencies (4–12 GHz).

B. Magnetization coupling

The temperature-dependent resonance field of the two modes observed in Fig. 1(e) is shown in detail in Fig. 2. At low temperatures the resonance field, H_0 , of the high-field mode increases, which differs from the behavior of the pure YIG crystal shown in Fig. 1(b). On the other hand, H_0 of the low-field mode shifts to the low-field side, and an anticrossing is observed. The mode anticrossing experimentally demonstrates the temperature-dependent magnetization coupling between YIG and GGG and can be predicted via the coupled LLG equations, as shown by the solid curves in Fig. 2 and discussed in detail below. The general nature of this temperature-dependent resonance-field anticrossing has also been observed in other YIG/GGG samples, indicating that this result is independent of the specific YIG/GGG bilayer design.

To describe the M_{YIG} - M_{GGG} coupling we write the interaction energy density as $U = -g\mu_0 \mathbf{M}_{YIG} \cdot \mathbf{M}_{GGG}$. Here g denotes the coupling coefficient, which depends on the dimensions of the YIG/GGG structure and the distance between M_{YIG} and M_{GGG} , with $g > 0$ indicating a ferromagnetic coupling and $g < 0$ indicating antiferromagnetic coupling. The interaction energy density produces an effective magnetization coupling field experienced by M_{YIG} , $\mu_0 \mathbf{H}_{\text{coupling}} = -\partial U / \partial \mathbf{M}_{YIG} = g\mu_0 \mathbf{M}_{GGG}$. With this coupling, the LLG equation for the YIG and GGG layer is

$$-\frac{d\mathbf{M}_{1,2}}{dt} = \mu_0 \gamma_{1,2} \mathbf{M}_{1,2} \times (\mathbf{H} + \mathbf{h}_{\text{rf}}) - \frac{\alpha_{1,2}}{M_{1,2}} \mathbf{M}_{1,2} \times \frac{d\mathbf{M}_{1,2}}{dt} + g\mu_0 \gamma_{1,2} \mathbf{M}_{1,2} \times \mathbf{M}_{2,1}, \quad (1)$$

where subscripts 1 and 2 represent the magnetizations of the YIG film and GGG substrate, respectively. Using Eq. (1) we have calculated the temperature dependence of the coupled YIG and GGG resonance fields, as indicated by the solid

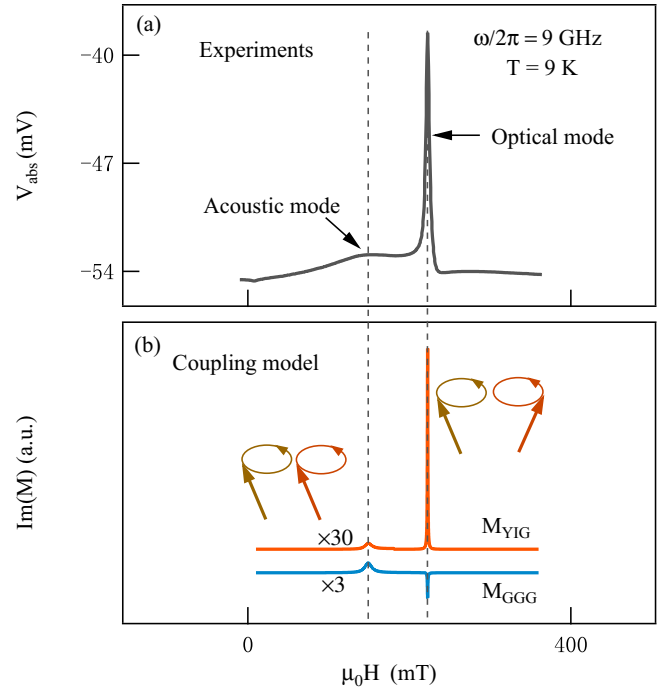


FIG. 3. Resonance signal from (a) experiment and (b) the magnetization coupling model. The red and blue solid lines correspond to the resonance signals given by M_{YIG} and M_{GGG} , respectively. The predicted acoustic resonance signal in M_{YIG} and M_{GGG} are magnified by a factor of 30 and a factor of 3, respectively. Here the microwave frequency is 9 GHz, and the temperature is 9 K.

lines in Fig. 2. In these calculations we used $\alpha_{GGG} = 0.036$, $\gamma_{GGG} = 2\pi \times 59$ GHz/T, and $\gamma_{YIG} = 2\pi \times 28$ GHz/T, which were measured in independent resonance experiments of YIG and GGG as described in Sec. III A. Typical literature values of α_{YIG} lie between 10^{-3} and 10^{-5} [8]. However the strongly coupled results of Fig. 2 are insensitive to the value of α_{YIG} within this range. Therefore in our calculations we have chosen to use $\alpha_{YIG} = 0.001$ [8]. Results identical to Fig. 2 can be obtained with any value in the range $10^{-5} < \alpha_{YIG} < 10^{-3}$. This calculation also incorporates the temperature dependence of M_{YIG} , which gradually decreases with increased temperature as $(1.6 \times 10^{-5} \text{ T})/K^{3/2}$ from a value of $\mu_0 M_{YIG} = 0.265$ T at $T = 0$ K. $M_{YIG}(T)$ was obtained by fitting the $M_{YIG}(T) - T$ relationship of the YIG/GGG optical resonance mode between 100 and 300 K. In this temperature range $M_{GGG} < 0.4$ mT and therefore the weak-coupling contribution to the resonance field of the YIG layer is negligible. A value of $\mu_0 M_{YIG} = 0.265$ T at 0 K is slightly larger than the reported value of 0.246 T found in the literature [38,40], which may be caused by the magnetic anisotropy. Therefore the anticrossing data of Fig. 2 has a single fitting parameter of $g = -0.08 < 0$, indicating an antiferromagnetic-type interaction between the YIG layer and GGG substrate.

Figures 3(a) and 3(b) show a typical magnetic resonance spectra, observed experimentally and calculated using the coupling model of Eq. (1), respectively, at a fixed microwave frequency of $\omega/2\pi = 9$ GHz. With the inclusion of magnetization coupling the resonance fields of the two modes given by the experiments and the coupling model are almost identical.

Furthermore the calculation shown in Fig. 3(b) allows us to identify the nature of the two coupled modes. The dip in M_{GGG} on the high-field side has a π phase shift from that of M_{YIG} , indicating that the high-field resonance signal in the YIG/GGG structure, shown in Fig. 3(a), corresponds to an optical mode, while an acoustic mode occurs on the low-field side where the M_{YIG} and M_{GGG} resonance are in phase.

C. Temperature-dependent amplitude and linewidth

Given the nature of the magnetization coupling in our model we expect the resonance amplitude L to be temperature dependent. This is verified by the data in Fig. 4(a), which shows L_{optical} and L_{acoustic} for the optical and acoustic modes as a function of temperature. From 300 to about 30 K L_{optical} is increasing, and begins to gradually decrease for $T < 30$ K. The solid curves in Fig. 4(a) are theoretical calculations of L_{optical} , with good agreement further verifying the magnetization coupling model. According to this description the behavior of L_{optical} is due to a competition between the temperature dependence of M_{YIG} and g . As T decreases from 300 to 30 K, the amplitude behavior is dominated by the increase of M_{YIG} , resulting in a growth of L_{optical} . However, as T continues to decrease below 30 K the large increase in magnetization coupling overtakes the growth of M_{YIG} , resulting in a decrease of L_{optical} . The experimental and theoretical results for the acoustic mode are also in qualitative agreement as shown in Fig. 4(a).

The controllable resonance field of the optical mode that is induced by the coupling, as shown in Fig. 2, is also observed in spin pumping measurements (not shown here). Interestingly the temperature dependence of the resonance linewidth, $\Delta H_{\text{optical}}$, is not fully explained by the magnetization coupling. More strikingly $\Delta H_{\text{optical}}$ also differs from the linewidth measured from spin pumping. Both $\Delta H_{\text{optical}}$ and the simultaneously measured ΔH_{SP} , extracted from spin pumping measurements [as shown in Fig. 4(b)], are summarized in Fig. 4(c). $\Delta H_{\text{optical}}$ and ΔH_{SP} exhibit qualitatively different behavior below 30 K, which may be related to the nature of magnetization coupling. This result means that the coupling effect appears different in FMR absorption and spin pumping measurements, although the resonance fields are almost identical in both measurements. Similar behavior has been observed at other microwave frequencies, and the mechanism is an interesting open question for further research.

D. Effective field due to magnetization coupling

Interlayer magnetization coupling results in an effective field, $\mu_0 \mathbf{H}_{\text{coupling}} = g\mu_0 \mathbf{M}_{GGG}$, which acts on M_{YIG} and can therefore manipulate the magnetization dynamics of the YIG layer. This effective field is further increased in high-frequency FMR experiments due to the increase of M_{GGG} at higher magnetic fields. Figure 5(a) shows the temperature-dependent FMR field at microwave frequencies from 4 to 12 GHz. An enhancement of $\mu_0 H_0$, induced by magnetization coupling, can be seen at all measured microwave frequencies, consistent with our expectations. To highlight this behavior we can estimate $\mu_0 H_{\text{coupling}}$ at 8 K by subtracting the weak-coupling contribution, $\mu_0 H_{\text{coupling}} \approx \mu_0 [H_0(8 \text{ K}) -$

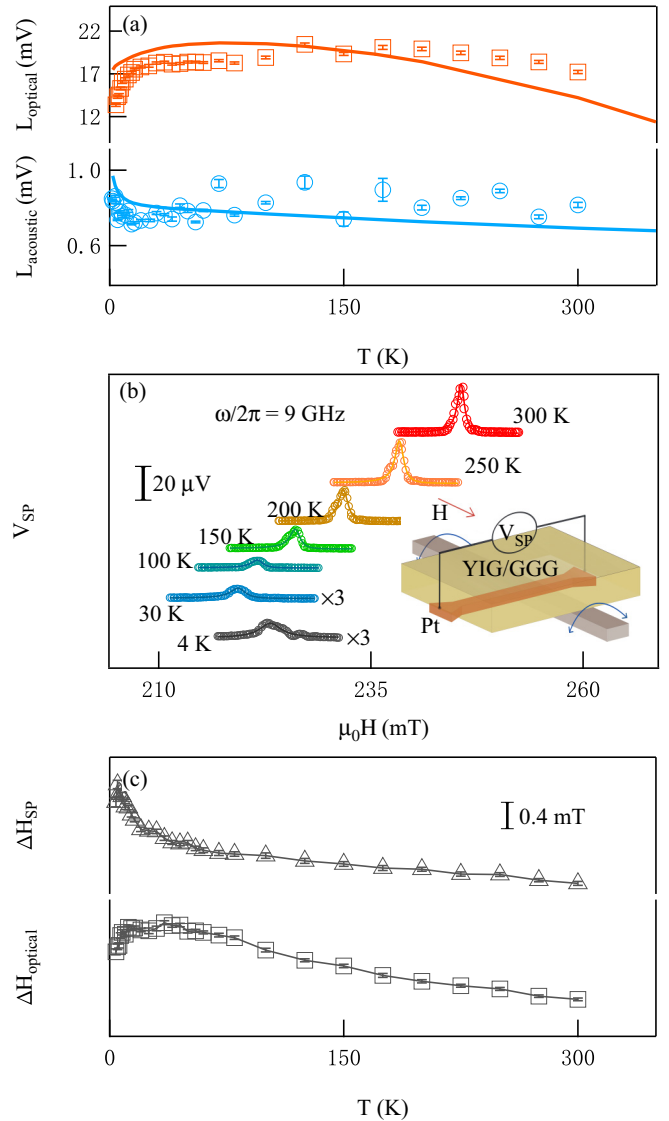


FIG. 4. (a) Resonance amplitudes L_{optical} and L_{acoustic} from the experiments and the coupling model are plotted as a function of temperature. (b) Waterfall plot of the spin pumping spectrum at various measurement temperatures. The spin pumping signal for $T = 30$ and 4 K are magnified by a factor of 3 for clarity. The inset shows the spin pumping measurement setup. (c) The temperature-dependent spin pumping (ΔH_{SP}) and optical mode ($\Delta H_{\text{optical}}$) linewidth in YIG/GGG. Here the microwave frequency is 9 GHz, and the line is a guide for the eyes.

$H_0(30 \text{ K})]$, as shown by the solid dots in Fig. 5(b). In this estimation we assume that $\mu_0 H_{\text{coupling}} \approx 0$ mT at 30 K due to the negligible paramagnetism of the GGG substrate relative to lower temperatures, as shown in Fig. 1(c). For comparison, $\mu_0 H_{\text{coupling}}$ can also be determined according to $g\mu_0 M_{GGG}$ from Eq. (1), which is linearly dependent on M_{GGG} for a fixed coupling coefficient g , as shown by the solid blue line in Fig. 5(b). Both $\mu_0 H_{\text{coupling}}$ and $\mu_0 [H_0(8 \text{ K}) - H_0(30 \text{ K})]$ increase with increasing microwave frequency due to the enhanced magnetic field used for higher frequency FMR experiments. The slope of $\mu_0 H_{\text{coupling}}$ and $\mu_0 [H_0(8 \text{ K}) - H_0(30 \text{ K})]$, with changing microwave frequency, is nearly

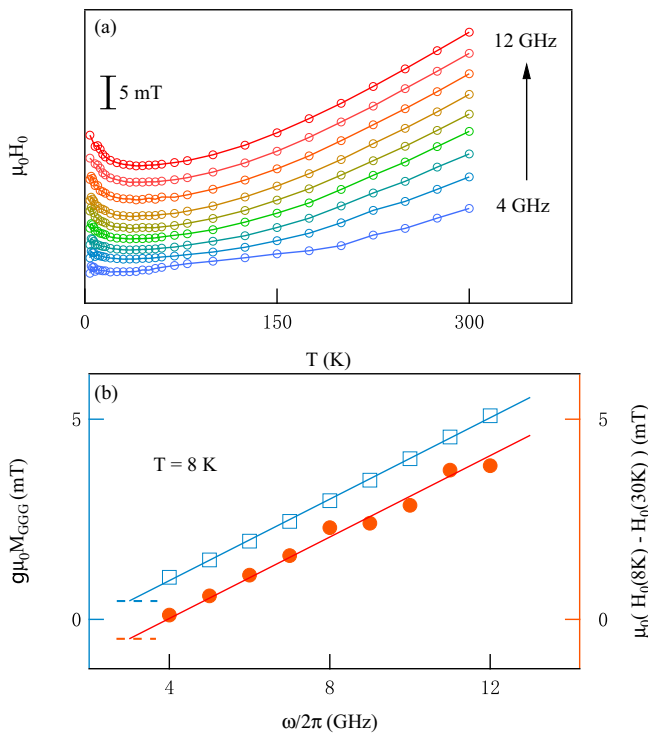


FIG. 5. (a) Temperature-dependent $\mu_0 H_0$ of the optical mode at various microwave frequencies. The resonance field is shifted to highlight the line shape at different frequencies. (b) Coupling effective field at 8 K from experiment and model.

identical [Fig. 5(b)], but there is an offset of about 1.48 mT at all measured frequencies due to the difference in M_{YIG} at 8 and 30 K. This shift is consistent with the temperature

dependence of the YIG FMR frequency shown in Fig. 1(b). In addition the effective field due to magnetization coupling can be enhanced by increasing M_{GGG} with higher magnetic field or lower temperature. Thus we have experimentally realized YIG magnon control via magnetization coupling in a YIG/GGG structure.

IV. CONCLUSION

In this work we experimentally studied the temperature-controlled magnetization coupling in a YIG/GGG structure. We found that the optical mode resonance field follows a different temperature dependence above and below $T = 30$ K, due to a competition between the temperature-dependent growth of M_{YIG} and the interlayer coupling. By analyzing the temperature-dependent antiferromagnetic-type interaction between YIG and GGG using the LLG equation we find that the magnetization dynamics of YIG are controlled via an effective coupling field induced by the magnetization coupling. Additionally the frequency and temperature-dependent magnetization coupling confirms that the effective field can be further enhanced by increasing the magnetic field and decreasing the temperature. Thus we have experimentally demonstrated temperature and field control of YIG magnons via YIG/GGG coupling, which will benefit the design of future magnonic devices.

ACKNOWLEDGMENTS

This work is supported by the National Natural Science Foundation of China (NSFC No. 11774200), the Shandong Provincial Natural Science Foundation (Grant No. ZR2019JQ02) and the Youth Interdisciplinary Science and Innovative Research Groups of Shandong University.

- [1] A. V. Chumak, V. I. Vasyuchka, A. A. Serga, and B. Hillebrands, Magnon spintronics, *Nat. Phys.* **11**, 453 (2015).
- [2] L. J. Cornelissen, J. Liu, R. A. Duine, J. Ben Youssef, and B. J. van Wees, Long-distance transport of magnon spin information in a magnetic insulator at room temperature, *Nat. Phys.* **11**, 1022 (2015).
- [3] A. V. Chumak, A. A. Serga, and B. Hillebrands, Magnon transistor for all-magnon data processing, *Nat. Commun.* **5**, 4700 (2014).
- [4] K. Vogt, F. Y. Fradin, J. E. Pearson, T. Sebastian, S. D. Bader, B. Hillebrands, A. Hoffmann, and H. Schultheiss, Realization of a spin-wave multiplexer, *Nat. Commun.* **5**, 3727 (2014).
- [5] L. J. Cornelissen, K. J. H. Peters, G. E. W. Bauer, R. A. Duine, and B. J. van Wees, Magnon spin transport driven by the magnon chemical potential in a magnetic insulator, *Phys. Rev. B* **94**, 014412 (2016).
- [6] B. L. Giles, Z. Yang, J. S. Jamison, and R. C. Myers, Long-range pure magnon spin diffusion observed in a nonlocal spin-Seebeck geometry, *Phys. Rev. B* **92**, 224415 (2015).
- [7] A. A. Serga, A. V. Chumak, and B. Hillebrands, YIG magnonics, *J. Phys. D: Appl. Phys.* **43**, 264002 (2010).
- [8] G. Schmidt, C. Hauser, P. Trempler, M. Paleschke, and E. Th. Papaioannou, Ultra thin films of yttrium iron garnet with very low damping: A review, *Phys. Status Solidi B* **257**, 1900644 (2020).
- [9] C. Liu, J. Chen, T. Liu, F. Heimbach, H. Yu, Y. Xiao, J. Hu, M. Liu, H. Chang, T. Stueckler, S. Tu, Y. Zhang, Y. Zhang, P. Gao, Z. Liao, D. Yu, K. Xia, N. Lei, W. Zhao, and M. Wu, Long-distance propagation of short-wavelength spin waves, *Nat. Commun.* **9**, 738 (2018).
- [10] J. Chen, T. Yu, C. Liu, T. Liu, M. Madami, K. Shen, J. Zhang, S. Tu, Md S. Alam, K. Xia, M. Wu, G. Gubbiotti, Y. M. Blanter, G. E. W. Bauer, and H. Yu, Excitation of unidirectional exchange spin waves by a nanoscale magnetic grating, *Phys. Rev. B* **100**, 104427 (2019).
- [11] J. Chen, C. Wang, C. Liu, S. Tu, L. Bi, and H. Yu, Spin wave propagation in ultrathin magnetic insulators with perpendicular magnetic anisotropy, *Appl. Phys. Lett.* **114**, 212401 (2019).
- [12] H. Wu, L. Huang, C. Fang, B. S. Yang, C. H. Wan, G. Q. Yu, J. F. Feng, H. X. Wei, and X. F. Han, Magnon Valve Effect between Two Magnetic Insulators, *Phys. Rev. Lett.* **120**, 097205 (2018).
- [13] C. Y. Guo, C. H. Wan, X. Wang, C. Fang, P. Tang, W. J. Kong, M. K. Zhao, L. N. Jiang, B. S. Tao, G. Q. Yu, and X. F. Han, Magnon valves based on YIG/NiO/YIG all-insulating magnon junctions, *Phys. Rev. B* **98**, 134426 (2018).

- [14] C. W. Sandweg, Y. Kajiwara, A. V. Chumak, A. A. Serga, V. I. Vasyuchka, M. B. Jungfleisch, E. Saitoh, and B. Hillebrands, Spin Pumping by Parametrically Excited Exchange Magnons, *Phys. Rev. Lett.* **106**, 216601 (2011).
- [15] H. Huebl, C. W. Zollitsch, J. Lotze, F. Hocke, M. Greifenstein, A. Marx, R. Gross, and S. T. B. Goennenwein, High Cooperativity in Coupled Microwave Resonator Ferrimagnetic Insulator Hybrids, *Phys. Rev. Lett.* **111**, 127003 (2013).
- [16] Y. Tabuchi, S. Ishino, T. Ishikawa, R. Yamazaki, K. Usami, and Y. Nakamura, Hybridizing Ferromagnetic Magnons and Microwave Photons in the Quantum Limit, *Phys. Rev. Lett.* **113**, 083603 (2014).
- [17] X. Zhang, C.-L. Zou, L. Jiang, and H. X. Tang, Strongly Coupled Magnons and Cavity Microwave Photons, *Phys. Rev. Lett.* **113**, 156401 (2014).
- [18] L. Bai, M. Harder, Y. P. Chen, X. Fan, J. Q. Xiao, and C.-M. Hu, Spin Pumping in Electrodynamically Coupled Magnon-Photon Systems, *Phys. Rev. Lett.* **114**, 227201 (2015).
- [19] Y.-P. Wang, G.-Q. Zhang, D. Zhang, T.-F. Li, C.-M. Hu, and J. Q. You, Bistability of Cavity Magnon Polaritons, *Phys. Rev. Lett.* **120**, 057202 (2018).
- [20] L. McKenzie-Sell, J. Xie, C.-M. Lee, J. W. A. Robinson, C. Ciccarelli, and J. A. Haigh, Low-impedance superconducting microwave resonators for strong coupling to small magnetic mode volumes, *Phys. Rev. B* **99**, 140414(R) (2019).
- [21] Y. Li, T. Polakovic, Y.-L. Wang, J. Xu, S. Lendinez, Z. Zhang, J. Ding, T. Khaire, H. Saglam, R. Divan, J. Pearson, W.-K. Kwok, Z. Xiao, V. Novosad, A. Hoffmann, and W. Zhang, Strong Coupling between Magnons and Microwave Photons in On-Chip Ferromagnet-Superconductor Thin-Film Devices, *Phys. Rev. Lett.* **123**, 107701 (2019).
- [22] J. T. Hou and L. Liu, Strong Coupling between Microwave Photons and Nanomagnet Magnons, *Phys. Rev. Lett.* **123**, 107702 (2019).
- [23] S. Klingler, V. Amin, S. Geprgs, K. Ganzhorn, H. Maier-Flaig, M. Althammer, H. Huebl, R. Gross, Robert D. McMichael, Mark D. Stiles, Sebastian T. B. Goennenwein, and M. Weiler, Spin-Torque Excitation of Perpendicular Standing Spin Waves in Coupled YIG/Co Heterostructures, *Phys. Rev. Lett.* **120**, 127201 (2018).
- [24] J. Chen, C. Liu, T. Liu, Y. Xiao, K. Xia, G. E. W. Bauer, M. Wu, and H. Yu, Strong Interlayer Magnon-Magnon Coupling in Magnetic Metal-Insulator Hybrid Nanostructures, *Phys. Rev. Lett.* **120**, 217202 (2018).
- [25] D. MacNeill, J. T. Hou, D. R. Klein, P. Zhang, P. Jarillo-Herrero, and L. Liu, Gigahertz Frequency Antiferromagnetic Resonance and Strong Magnon-Magnon Coupling in the Layered Crystal CrCl_3 , *Phys. Rev. Lett.* **123**, 047204 (2019).
- [26] L. Liensberger, A. Kamra, H. Maier-Flaig, S. Geprägs, A. Erb, S. T. B. Goennenwein, R. Gross, W. Belzig, H. Huebl, and M. Weiler, Exchange-Enhanced Ultrastrong Magnon-Magnon Coupling in a Compensated Ferrimagnet, *Phys. Rev. Lett.* **123**, 117204 (2019).
- [27] C. Dubs, O. Surzhenko, R. Linke, A. Danilewsky, U. Brückner, and J. Dellith, Sub-micrometer yttrium iron garnet LPE films with low ferromagnetic resonance losses, *J. Phys. D: Appl. Phys.* **50**, 204005 (2017).
- [28] Y. Sun, Y.-Y. Song, H. Chang, M. Kabatek, M. Jantz, W. Schneider, M. Wu, H. Schultheiss, and A. Hoffmann, Growth and ferromagnetic resonance properties of nanometer-thick yttrium iron garnet films, *Appl. Phys. Lett.* **101**, 152405 (2012).
- [29] I. H. Solt, Jr., Temperature dependence of YIG magnetization, *J. Appl. Phys.* **33**, 1189 (1962).
- [30] H. L. Wang, C. H. Du, Y. Pu, R. Adur, P. C. Hammel, and F. Y. Yang, Scaling of Spin Hall Angle in 3d, 4d, and 5d Metals from $\text{Y}_3\text{Fe}_5\text{O}_{12}$ /Metal Spin Pumping, *Phys. Rev. Lett.* **112**, 197201 (2014).
- [31] Y. Kajiwara, K. Harii, S. Takahashi, J. Ohe, K. Uchida, M. Mizuguchi, H. Umezawa, H. Kawai, K. Ando, K. Takanashi, S. Maekawa, and E. Saitoh, Transmission of electrical signals by spin-wave interconversion in a magnetic insulator, *Nature (London)* **464**, 262 (2010).
- [32] V. Castel, N. Vlietstra, J. B. Youssef, and B. J. van Wees, Platinum thickness dependence of the inverse spin-Hall voltage from spin pumping in a hybrid yttrium iron garnet/platinum system, *Appl. Phys. Lett.* **101**, 132414 (2012).
- [33] L. C. Hsia, H. Reimann, and P. E. Weign, Effect of temperature on magnetostatic mode spectra of reduced Ca-doped YIG thin films, *IEEE Trans. Magn.* **17**, 2961 (1981).
- [34] V. V. Danilov, D. L. Lyfar', Yu. V. Lyubon'ko, A. Yu. Nechiporuk, and S. M. Ryabchenko, Low-temperature ferromagnetic resonance in epitaxial garnet films on paramagnetic substrates, *Sov. Phys. J.* **32**, 276 (1989).
- [35] I. Laulicht and J. T. Suss, The temperature dependence of the ferromagnetic and paramagnetic resonance spectra in thin yttrium-iron-garnet films, *J. Appl. Phys.* **70**, 2251 (1991).
- [36] W.-C. Chianga, M. Y. Chernb, J. G. Linc, and C. Y. Huang, FMR studies of $\text{Y}_3\text{Fe}_5\text{O}_{12}/\text{Gd}_3\text{Ga}_5\text{O}_{12}$ (YIG/GGG), *J. Magn. Magn. Mater.* **239**, 332 (2002).
- [37] C. L. Jermain, S. V. Aradhya, N. D. Reynolds, R. A. Buhrman, J. T. Brangham, M. R. Page, P. C. Hammel, and F. Y. Yang, Increased low-temperature damping in yttrium iron garnet thin films, *Phys. Rev. B* **95**, 174411 (2017).
- [38] H. Maier-Flaig, S. Klingler, C. Dubs, O. Surzhenko, R. Gross, M. Weiler, H. Huebl, and S. T. B. Goennenwein, Temperature-dependent magnetic damping of yttrium iron garnet spheres, *Phys. Rev. B* **95**, 214423 (2017).
- [39] C. Kittel, On the theory of ferromagnetic resonance absorption, *Phys. Rev.* **73**, 155 (1948).
- [40] D. D. Stancil and A. Prabhakar, *Spin Waves: Theory and Applications* (Springer, US, 2009), pp. 333–334.